

Gluonic three-point correlations in pure Landau gauge QCD

Adrian Lorenz Blum,¹ Markus Q. Huber,¹ Mario Mitter,² and Lorenz von Smekal^{1,3}

¹*Theoriezentrum, Institut für Kernphysik, Technische Universität Darmstadt, 64289 Darmstadt, Germany*

²*Institut für Theoretische Physik, Ruprecht-Karls-Universität, 69120 Heidelberg, Germany*

³*Institut für Theoretische Physik, Justus-Liebig-Universität, 35392 Gießen, Germany*

(Dated: March 28, 2014)

We report on the first self-consistent solution of the Dyson-Schwinger equation (DSE) for the three-gluon vertex. Based on earlier results for the propagators which match data from lattice Monte-Carlo simulations, we obtain results for the three-gluon vertex that are in very good agreement with available lattice data likewise. Feeding these results back into the propagator DSEs leads to some changes especially in the gluon propagator. These changes allow us to assess previously used models for the three-gluon vertex and to systematically estimate the influence of neglected two-loop diagrams with four-gluon interactions. In the final step, a full iterative solution to the coupled DSEs of pure Landau gauge QCD without quarks is then obtained for the first time in an extended truncation which now dynamically includes the complete set of three-point vertex functions.

PACS numbers: 12.38.Aw, 14.70.Dj, 12.38.Lg

Introduction. The correlation functions of quantum chromodynamics (QCD) are the fundamental building blocks for hadron phenomenology [1] and strong-interaction matter studies based on functional continuum methods [2]. Built on a solid understanding of the pure gauge theory's vacuum correlations [3–7], there has recently been considerable progress in extensions to finite temperature [8–10], to including dynamical quarks [11–13], and to finite baryon density with all three light quark flavors included [14]. Via corresponding calculations of Polyakov-loop potentials [15], which have recently also included unquenching [16, 17] and quark matter effects [18], they also provide input for Polyakov-loop extended quark [19] and quark-meson models [20].

In this paper we go back to the foundations and consider pure Landau gauge QCD without quarks, for which the correlation functions have been intensely studied within a variety of approaches. These range from Monte-Carlo simulations on discrete space-time lattices to functional continuum methods such as Dyson-Schwinger equations (DSEs) or Functional Renormalization Group studies. Thereby, good qualitative agreement has been achieved since lattice sizes have become large enough to access the deep infrared (IR), far below the scale of QCD, Λ_{QCD} , in simulations [21–24]. At intermediate momenta, of the order of Λ_{QCD} , where much of the non-perturbative dynamics relevant to hadron physics happens, however, there are still some quantitative discrepancies. Especially in view of applying functional continuum methods to strong-interaction matter at finite baryon density, where the fermion sign problem is impeding direct lattice simulations, it is worthwhile to resolve these discrepancies. The QCD vacuum correlations thus serve as an important benchmark before the distinctive feature of functional methods to be readily extensible to finite baryon density can fully and reliably be exploited.

Moreover, a key role in hadron physics and finite density applications is increasingly being played by 3- and higher n -point vertex functions. Even for the 3-point

vertex functions, however, lattice data is rather limited, see [25–27]. This is to some extent due to their more complicated kinematics. Typically, lattice data has therefore so far only become available for very restricted kinematical configurations. While such restricted data provides valuable constraints, functional methods can also fill this gap and yield kinematically complete descriptions.

On the other hand, the infinite sets of functional equations for correlation functions require truncations. In the past this basically always meant that model input was used for the 3-point vertex functions to self-consistently solve non-linear functional equations for the propagators [6, 28–32]. While such 2-point complete truncations are nowadays being extended into the complex invariant momentum plane, e.g., for direct calculations of the corresponding spectral functions [33], the fully self-consistent inclusion of dynamic 3-point vertex functions has only started very recently [7, 34]. Despite constituting a major conceptual breakthrough the structurally simplest of all QCD vertex functions, the ghost-gluon vertex, was thereby shown to only have a minor quantitative influence on the propagators [7] as predicted [4] and confirmed in [35]. In contrast, it is usually argued that the three-gluon vertex plays a crucial role in the mid-momentum regime around Λ_{QCD} . The limited lattice data available for this vertex [26], however, left considerable room for speculations and models that had to be used in the past. Recently also perturbative calculations with a Curci-Ferrari mass term were done [36] that describe the qualitative features of the vertex quite well.

In this paper we present the next major step which is to also include the three-gluon vertex fully self-consistently and dynamically in a DSE solution for the pure gauge theory which is thus now 3-point complete for the first time. Before that, however, we first describe a standalone solution to a truncated three-gluon vertex DSE based on input propagators from [7] that are in very good agreement with lattice data. The fact that this standalone solution is then in turn consistent with the available lattice

data for the three-gluon vertex confirms the validity of our truncation of this DSE. Feeding the lattice-consistent three-gluon vertex back into the propagator DSEs serves to demonstrate to what extent the previously used model vertex [7] effectively includes contributions from the neglected two-loop diagrams in the gluon propagator DSE. The final step then is the fully iterated solution to the 3-point complete set of propagator *and* vertex DSEs, now based on a four-gluon vertex model. While the iteration has some effect on the three-gluon vertex, it hardly changes the propagators anymore which is encouraging evidence of convergence of this type of vertex expansion.

Computational scheme. The general setup follows that of Ref. [7] where the coupled system of ghost-gluon vertex and propagator DSEs was solved. The Landau gauge gluon and ghost propagators are parameterized by two invariant functions (color indices suppressed),

$$D_{\mu\nu}^A(p) = P_{\mu\nu}(p) \frac{Z(p^2)}{p^2} \quad \text{and} \quad D^c(p) = -\frac{G(p^2)}{p^2}, \quad (1)$$

where $P_{\mu\nu}(p)$ is the transverse projector. In the Landau gauge, the relevant transverse part of the three-gluon vertex can be written in terms of four independent Lorentz tensors. Including a complete basis for this tensor structure in the three-gluon vertex DSE, one can show, however, that the transverse part of the tree-level structure provides the dominant contribution to the full three-gluon vertex [37]. In our present study, we therefore maintain only this tree-level structure in the ansatz,

$$\Gamma_{\mu\nu\rho}^{A^3,abc}(p, q, k) = i g f^{abc} D^{A^3}(p^2, q^2, \alpha) ((q-p)_\rho g_{\mu\nu} + \text{perm.}), \quad (2)$$

where α is the angle between momenta p and q . To project the three-gluon vertex DSE onto this structure we contract it with three transverse projectors and a tree-level three-gluon vertex, for which $D^{A^3} \equiv 1$, as it is also done in lattice calculations [26]. One advantage of this procedure is that the same projection occurs in the gluon loop of the gluon propagator DSE. Consequently, the error induced in the gluon DSE by this restriction can be quantified from comparing the so projected vertex DSE results with analogously projected lattice data.

The full three-gluon vertex DSE, whose diagrammatic form can be found in Ref. [38] for example, is truncated by discarding all explicit two-loop diagrams together with a diagram that contains an irreducible ghost-gluon scattering kernel without tree-level counterpart. The resulting truncation is shown diagrammatically in Fig. 1. It is complete at leading order in the ultraviolet (UV). Moreover, it also includes the IR dominant contribution given by the ghost triangle, so that truncation errors should manifest themselves only in the mid-momentum region. To obtain a Bose symmetric result, the DSE is finally symmetrized by averaging over all three possible positions of the bare vertex in the diagrams.

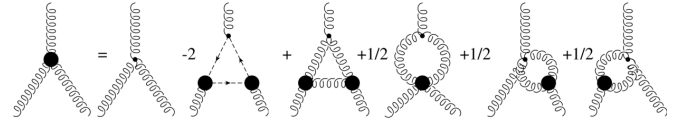


Figure 1: Truncated three-gluon vertex DSE with (dashed) ghost and (wiggly) gluon triangles, plus so-called swordfish diagrams with 4-point interactions. Solid black disks represent dressed vertices. Propagators inside loops are also dressed.

For renormalization we use the *MiniMOM* scheme [39], i.e., minimal subtraction of the ghost-gluon vertex (which entails $\tilde{Z}_1 = 1$ in Landau gauge) combined with momentum subtraction for the propagators. The renormalization constant of the three-gluon vertex is then fixed by its Slavnov-Taylor identity, $Z_1 = Z_3/\tilde{Z}_3$, where Z_3 and \tilde{Z}_3 are the renormalization constants of gluon and ghost fields, respectively. Z_1 and Z_4 factors also come with the tree-level vertices in gluon loops. To reproduce correct anomalous dimensions, we have to replace them by momentum dependent factors there [29]. Our construction of Z_1 for this renormalization group improvement is described in Ref. [7]. For Z_4 we use analogously,

$$Z_4 \rightarrow D_{RG}^{A^4}(p, q, r, s) = G(\bar{p}^2)^{\alpha_{4g}} Z(\bar{p}^2)^{\beta_{4g}}, \quad (3)$$

where $\bar{p}^2 = (p^2 + q^2 + r^2 + s^2)/2$. The exponents α_{4g} and β_{4g} are then determined from the leading anomalous dimension of the four-gluon vertex, $\gamma_{4g} = 2/11$, and from the requirement that the vertex approaches a constant value in the IR. These two conditions together yield $\alpha_{4g} = -8/9$ and $\beta_{4g} = 0$.

Note that there is no freedom in the subtraction of the three-gluon vertex DSE because this would in general violate the Slavnov-Taylor identity and hence be inconsistent with the MiniMOM scheme. Its overall strength can therefore not be adjusted manually by renormalization. In general one observes, however, that the iteration of the three-gluon vertex DSE with fixed propagator input, roughly comparable to lattice data, does not converge once three-gluon interactions of a certain strength build up [52]. Because of cancellations between the gluon triangle, where these enter quadratically, and the swordfish diagrams, with four-gluon interactions, this can at present only be avoided by using a sufficiently strong four-gluon vertex as model input [37]. Especially its strength in the mid-momentum regime is thereby important for the balance between gluon triangle and swordfish diagrams. This suggests that the neglected UV-subleading contributions and tensor structures might have a similar effect in the full DSE. It is thus in line with our general strategy for the vertex expansion that such higher-order effects are compensated by the model input for the 4-point interactions used to close the 3-point complete system of DSEs. The situation is analogous to that in previous 2-point complete truncations, where models for the three-gluon vertex were also partially constrained by the convergence of the gluon propagator DSE solution.

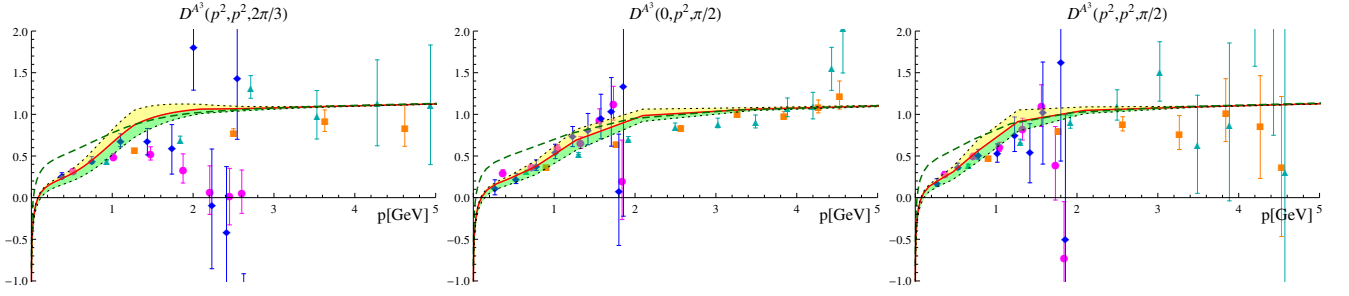


Figure 2: Three-gluon vertex dressing function with restricted kinematics (see legends) for comparison with lattice data where different colors/symbols refer to different values of $\beta \in \{2.2, 2.5\}$ and different lattice sizes $1.4 \text{ fm} < L < 4.7 \text{ fm}$, see [26] for details. Solid red line: standalone solution with $a = 1.5$ and $b = 1.95 \text{ GeV}^2$. Upper (yellow) band: variation with b down to 1.46 GeV^2 . Lower (green) band: strengths up to $a = 2$. Green dashed line: solution to fully coupled system ($a = 1.5$, $b = 1.94 \text{ GeV}^2$).

We again use a tree-level ansatz for the Lorentz and color structure of the dressed four-gluon vertex. To enhance its low and mid-momentum strength as compared to the form in Eq. (3) we use a two parameter ansatz for its dressing,

$$D^{A^4}(p, q, r, s) = (a \tanh(b/\bar{p}^2) + 1) D_{RG}^{A^4}(p, q, r, s), \quad (4)$$

where a determines the additional IR interaction strength and b the momentum scale of its onset. Qualitatively, such an enhancement is in fact in agreement with a first exploratory study of the four-gluon vertex function [40].

As in Ref. [7], where further technical details are found, the program *DoFun* [41, 42] was used to derive the DSEs and the *CrasyDSE* framework [43] for their solution.

Standalone three-gluon vertex. With the ghost-gluon vertex and the propagators from [7] as fixed input which agrees with lattice data very well, see, e.g., the dashed blue line for the gluon propagator in Fig. 4, the calculation of the three-gluon vertex serves as a test of its truncated DSE with simplified tensor structure and the four-gluon vertex model (4). In Fig. 2 we compare the resulting dressing function $D^{A^3}(p^2, q^2, \alpha)$ defined in Eq. (2)

for the symmetric momentum configuration $k^2 = p^2 = q^2$ (left) and for two orthogonal configurations with $p \cdot q = 0$, for $k^2 = p^2$ (middle) and $q^2 = p^2$ (right), to the lattice data of Ref. [26]. A rather good description of the lattice data is obtained for an IR strength parameter $a \approx 1.5$ with an onset around $b \approx 2 \text{ GeV}^2$ in the four-gluon vertex model. Varying its strength and onset by about 30% leads to the bands used in the figure to indicate the sensitivity to these model parameters. The four-gluon vertex model thus appears to compensate the mid-momentum contributions from neglected diagrams in the tree-level projected three-gluon vertex DSE quite well.

As already observed in [7], our results for the three-gluon vertex function change sign at very low momenta. The position of this zero crossing in our calculations for the momentum configurations of Fig. 2 varies roughly between 80 and 100 MeV, typically with a 20% variation over the bands. Our larger value, which is obtained for the configuration in the middle, is thereby reasonably close to a previous estimate of about 130 MeV [44]. With the available lattice sizes this zero crossing has not yet been accessible by Monte-Carlo simulations in four dimensions. It has been observed, however, by simulations on larger lattices in two [45] and three dimensions [26], where it was confirmed by DSE studies [38, 46].

For even lower momenta our results for the three-gluon vertex function furthermore show a logarithmic behavior with signs of a divergence at vanishing momenta. For the momentum configuration in the middle of Fig. 2, such a logarithmic divergence has also been predicted in [44]. It agrees with the general arguments of Ref. [47], and it has been seen explicitly in a recent perturbative calculation with Curci-Ferrari mass term as well [36].

Strictly speaking, the lattice data shown here was obtained for the pure $SU(2)$ gauge theory, while our DSE calculations refer to $SU(3)$. At the present accuracy level, this difference is not significant, however. The renormalized propagators of the two basically coincide [23]. For completeness we provide corresponding DSE results for $SU(2)$, which indeed compare equally well with the lattice data, in the Supplemental Material.

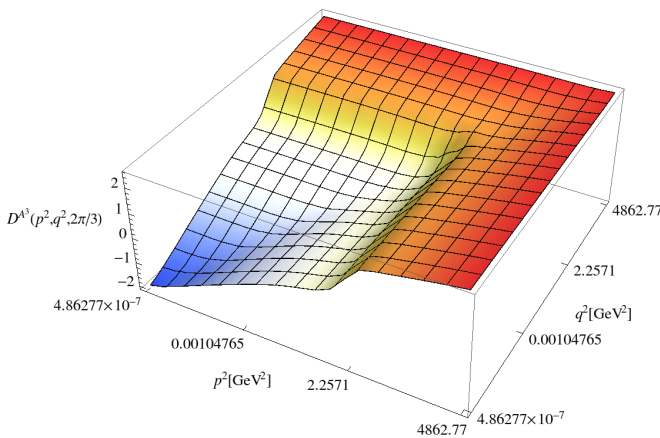


Figure 3: Three-gluon vertex dressing function for $\alpha = 2\pi/3$.

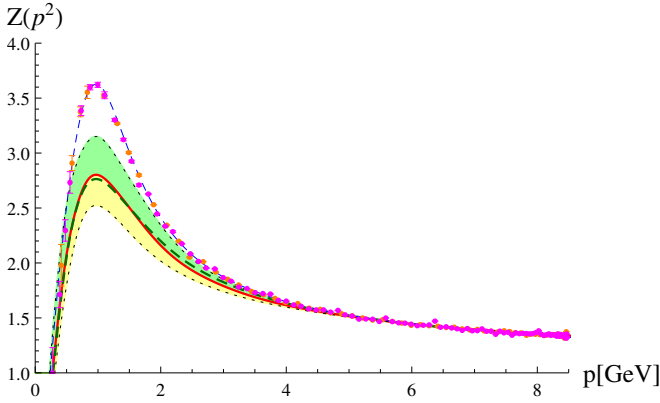


Figure 4: Gluon dressing function from [7] (dashed blue), with lattice data from [50], compared to analogous calculations with the three-gluon vertices shown as the bands around the solid red line in Fig. 2 and the same color coding here. Iterating the full 3-point complete set of DSEs then changes the center of the band (solid red) into the dashed green line.

A typical example of how our results extend the lattice data in Fig. 2, here with $\alpha = 2\pi/3$ (left), to general kinematics is shown in Fig. 3. Analogous $SU(2)$ results and further examples are given in the Supplemental Material.

Gluon propagator. As mentioned above, the way we project the three-gluon vertex DSE onto the tree-level structure (2) leads to the same structure that also occurs inside the gluon loop of the gluon propagator DSE. Using in this DSE a three-gluon vertex for which this same structure resembles lattice data therefore practically eliminates the effects of other tensor structures on the gluon propagator, which is shown in Fig. 4. Solving its DSE with the three-gluon vertices shown as the bands in Fig. 2 reduces the result of [7] (dashed blue), i.e., the input for these vertex DSE solutions, to the corresponding bands around the solid red line here. Since these three-gluon vertices agree within errors with the lattice data, the missing strength of the gluon propagator in the mid-momentum regime has to come from the neglected two-loop diagrams which hence deserve further study. For first results see [48, 49]. Ghost propagator and $SU(2)$ results are given in the Supplemental Material.

Full 3-point complete solution. We have seen that with proper input our standalone three-gluon vertex DSE solution agrees well with lattice data. Using this solution in the gluon propagator DSE exposes missing contributions there. The resulting gluon propagator decreases at mid-momentum and no longer agrees with lattice data. If we feed this result back into the vertex DSE, it is thus to be expected that its agreement with lattice data deteriorates, likewise. This is indeed the case as seen in Fig. 2 where the dashed green lines show the iterated and converged solution for the three-gluon vertex from the 3-point complete system of propagator and 3-point vertex DSEs. Apart from the expected deviations, these fully self-consistent results are otherwise stable, however.

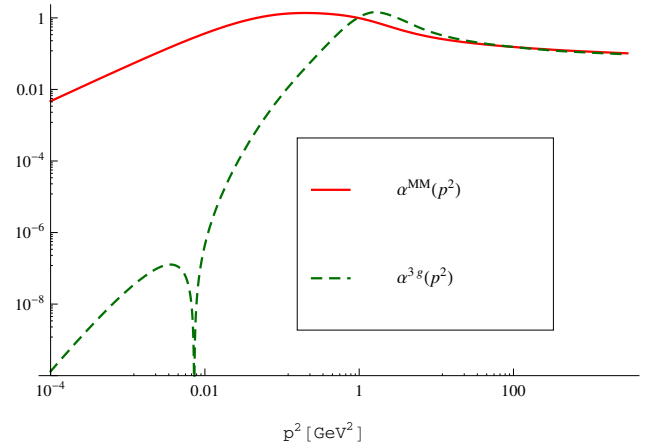


Figure 5: Comparison of couplings as defined via ghost-gluon (solid red) and three-gluon (dashed green) vertex.

In particular, it is quite reassuring for the convergence of this kind of vertex expansion that the propagators remain almost unaffected by these deviations in the three-gluon vertex as can be seen, for example, in the gluon propagator upon comparing the solid red line of Fig. 4, from the lattice consistent vertex, with the dashed green fully iterated result, corresponding to the fully iterated dashed green vertex result in Fig. 2.

The ghost propagator and ghost-gluon vertex are both affected very little by the inclusion of the three-gluon vertex in the 3-point complete iteration and are not shown here.

Running couplings. The MiniMOM coupling is defined by minimal subtraction of the ghost-gluon vertex, i.e., in Landau gauge as $\alpha^{\text{MM}}(p^2) = \alpha(\mu^2)Z(p^2)G(p^2)^2$ [28, 39]. Alternatively, one could of course also define a running coupling from the three-gluon vertex in a symmetric MOM scheme, for example, see Ref. [51],

$$\alpha^{3g}(p^2) = \alpha(\mu^2) \frac{Z(p^2)^3 D^{A^3}(p^2, p^2, 2\pi/3)^2}{Z(\mu^2)^3 D^{A^3}(\mu^2, \mu^2, 2\pi/3)^2}. \quad (5)$$

The denominator herein, which would be unity with subtracting at $p^2 = \mu^2$ in such a symmetric MOM scheme, is used to convert our Z and D^{A^3} from the MiniMOM scheme to this scheme. For μ far enough in the perturbative regime the two couplings must agree in the UV. A comparison is given in Fig. 5. Because of the zero crossing in the three-gluon vertex, $\alpha^{3g}(p^2)$ has a zero at non-vanishing momentum likewise. This is not prohibited, in general, for a renormalization group invariant dimensionless function of a single scale which reduces to the perturbative running coupling in the UV, but it does certainly go against the common notion of a running coupling.

Summary and conclusions. We have shown how a truncated DSE for the three-gluon vertex with appropriate input and modeling of four-gluon interactions can

produce reliable results which stand the test against current lattice data. Using these results in the gluon propagator DSE, we could clearly identify missing contributions in the mid-momentum regime around 1 GeV as being due to neglected two-loop diagrams therein. Our solid results for the three-gluon vertex will help to include these diagrams in the future. Meanwhile we have solved for the first time a coupled system of DSEs for propagators *and* vertex functions that is complete on the level of 3-point correlations with model 4-point interactions. The fully self-consistent results from this 3-point complete truncation show clear signs of convergence of

the underlying vertex expansion for QCD.

Acknowledgments. We would like to thank Reinhard Alkofer, Gernot Eichmann, Christian S. Fischer, Leonard Fister, Axel Maas, Jan M. Pawłowski, Andre Sternbeck, and Richard Williams for helpful discussions. This work was supported by the Helmholtz International Center for FAIR within the LOEWE program of the State of Hesse, the European Commission, FP7-PEOPLE-2009-RG No. 249203, the Alexander von Humboldt foundation and the BMBF grant OSPL2VHCTG.

-
- [1] G. Eichmann, *J.Phys.Conf.Ser.* **426** (2013) 012014.
 - [2] J. M. Pawłowski, *AIP Conf.Proc.* **1343** (2011) 75–80.
 - [3] R. Alkofer and L. von Smekal, *Phys. Rept.* **353** (2001) 281.
 - [4] C. Lerche and L. von Smekal, *Phys.Rev.* **D65** (2002) 125006.
 - [5] J. M. Pawłowski, D. F. Litim, S. Nedelko, and L. von Smekal, *Phys. Rev. Lett.* **93** (2004) 152002.
 - [6] C. S. Fischer, A. Maas, and J. M. Pawłowski, *Annals Phys.* **324** (2009) 2408–2437.
 - [7] M. Q. Huber and L. von Smekal, *JHEP* **1304** (2013) 149.
 - [8] C. S. Fischer, A. Maas, and J. A. Müller, *Eur.Phys.J.* **C68** (2010) 165–181.
 - [9] A. Maas, J. M. Pawłowski, L. von Smekal, and D. Spielmann, *Phys.Rev.* **D85** (2012) 034037.
 - [10] L. Fister and J. M. Pawłowski, [arXiv:1112.5440 \[hep-ph\]](#).
 - [11] J. Braun, L. M. Haas, F. Marhauser, and J. M. Pawłowski, *Phys. Rev. Lett.* **106** (2011) 022002.
 - [12] C. S. Fischer, J. Luecker, and J. A. Mueller, *Phys.Lett.* **B702** (2011) 438–441.
 - [13] R. Aouane, F. Burger, E.-M. Ilgenfritz, M. Muller-Preussker, and A. Sternbeck, *Phys.Rev.* **D87** (2013) 114502.
 - [14] C. S. Fischer and J. Luecker, *Phys.Lett.* **B718** (2013) 1036–1043.
 - [15] J. Braun, H. Gies, and J. M. Pawłowski, *Phys. Lett.* **B684** (2010) 262–267.
 - [16] L. Fister and J. M. Pawłowski, *Phys.Rev.* **D88** (2013) 045010.
 - [17] L. M. Haas, R. Stiele, J. Braun, J. M. Pawłowski, and J. Schaffner-Bielich, *Phys.Rev.* **D87** (2013) 076004.
 - [18] C. S. Fischer, L. Fister, J. Luecker, and J. M. Pawłowski, [arXiv:1306.6022 \[hep-ph\]](#).
 - [19] T. Hell, K. Kashiwa, and W. Weise, *Phys.Rev.* **D83** (2011) 114008.
 - [20] T. K. Herbst, M. Mitter, J. M. Pawłowski, B.-J. Schaefer, and R. Stiele, *Phys.Lett.* **B731** (2014) 248–256.
 - [21] A. Cucchieri and T. Mendes, *PoS LAT2007* (2007) 297.
 - [22] A. Cucchieri and T. Mendes, *Phys. Rev.* **D78** (2008) 094503.
 - [23] A. Sternbeck, L. von Smekal, D. Leinweber, and A. Williams, *PoS LAT2007* (2007) 340.
 - [24] I. L. Bogolubsky, E. M. Ilgenfritz, M. Müller-Preussker, and A. Sternbeck, *Phys. Lett.* **B676** (2009) 69–73.
 - [25] A. Kizilersu, D. B. Leinweber, J.-I. Skullerud, and A. G. Williams, *Eur.Phys.J.* **C50** (2007) 871–875.
 - [26] A. Cucchieri, A. Maas, and T. Mendes, *Phys. Rev.* **D77** (2008) 094510.
 - [27] E. M. Ilgenfritz, M. Müller-Preussker, A. Sternbeck, A. Schiller, and I. L. Bogolubsky, *Braz. J. Phys.* **37** (2007) 193.
 - [28] L. von Smekal, R. Alkofer, and A. Hauck, *Phys. Rev. Lett.* **79** (1997) 3591–3594.
 - [29] L. von Smekal, A. Hauck, and R. Alkofer, *Ann. Phys.* **267** (1998) 1.
 - [30] A. Aguilar, D. Binosi, and J. Papavassiliou, *Phys.Rev.* **D78** (2008) 025010.
 - [31] M. Pennington and D. Wilson, *Phys.Rev.* **D84** (2011) 119901.
 - [32] F. J. Llanes-Estrada and R. Williams, *Phys.Rev.* **D86** (2012) 065034.
 - [33] S. Strauss, C. S. Fischer, and C. Kellermann, *Phys.Rev.Lett.* **109** (2012) 252001.
 - [34] M. Hopfer and R. Alkofer, *Acta Phys.Polon.Supp.* **6** no. 3, (2013) 929–934.
 - [35] A. Aguilar, D. Ibáñez, and J. Papavassiliou, *Phys.Rev.* **D87** (2013) 114020.
 - [36] M. Pelaez, M. Tissier, and N. Wschebor, *Phys.Rev.* **D88** (2013) 125003.
 - [37] G. Eichmann, R. Williams, R. Alkofer, and M. Vujanovic, [arXiv:1402.1365 \[hep-ph\]](#).
 - [38] M. Q. Huber, A. Maas, and L. von Smekal, *JHEP* **1211** (2012) 035.
 - [39] L. von Smekal, K. Maltman, and A. Sternbeck, *Phys.Lett.* **B681** (2009) 336–342.
 - [40] C. Kellermann and C. S. Fischer, *Phys. Rev.* **D78** (2008) 025015.
 - [41] M. Q. Huber and J. Braun, *Comput.Phys.Commun.* **183** (2012) 1290–1320.
 - [42] R. Alkofer, M. Q. Huber, and K. Schwenzer, *Comput. Phys. Commun.* **180** (2009) 965–976.
 - [43] M. Q. Huber and M. Mitter, *Comput.Phys.Commun.* **183** (2012) 2441–2457.
 - [44] A. Aguilar, D. Binosi, D. Ibáñez, and J. Papavassiliou, [arXiv:1312.1212 \[hep-ph\]](#).
 - [45] A. Maas, *Phys. Rev.* **D75** (2007) 116004.
 - [46] D. R. Campagnari and H. Reinhardt, *Phys.Rev.* **D82** (2010) 105021.
 - [47] R. Alkofer, M. Q. Huber, and K. Schwenzer, *Phys. Rev.*

D81 (2010) 105010.

- [48] J. C. Bloch, *Few Body Syst.* **33** (2003) 111–152.
- [49] V. Mader and R. Alkofer, *PoS ConfinementX* (2012) 063.
- [50] A. Sternbeck, [arXiv:hep-lat/0609016](https://arxiv.org/abs/hep-lat/0609016), PhD thesis, Humboldt-Universität zu Berlin, 2006.
- [51] R. Alkofer, C. S. Fischer, and F. J. Llanes-Estrada, *Phys.Lett.* **B611** (2005) 279–288.
- [52] We thank G. Eichmann and R. Williams for bringing this to our attention, for numerical cross-checks, and for clarifying discussions on how to resolve the issue.

Supplemental Material

For completeness we show the ghost dressing function in Fig. 6. As expected, the effect of the three-gluon vertex is only minor since it enters only indirectly via the gluon propagator.

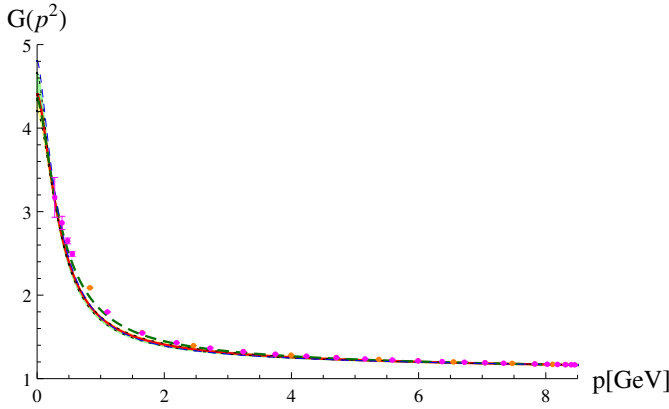


Figure 6: $SU(3)$ ghost dressing functions: Input from [7] depicted by a dashed blue line. Results from standalone solution to three-gluon vertex DSE shown as solid red line (with hardly visible small bands corresponding to those in Figs. 2 and 4), and iterated solution from the 3-point complete truncation as dashed green line, with lattice data from Ref. [50].

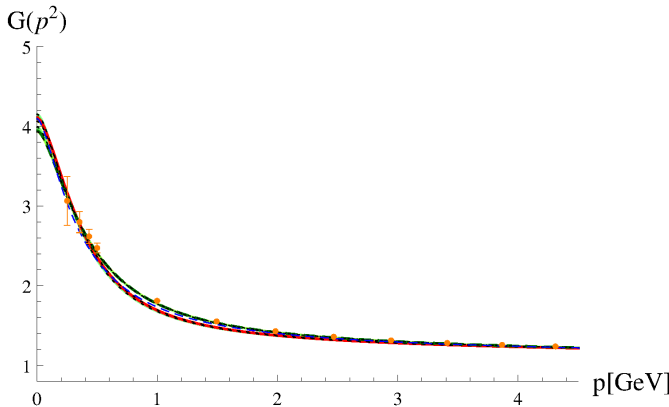


Figure 7: $SU(2)$ ghost dressing functions with lattice data from [23] corresponding to those shown for $SU(3)$ in Fig. 6.

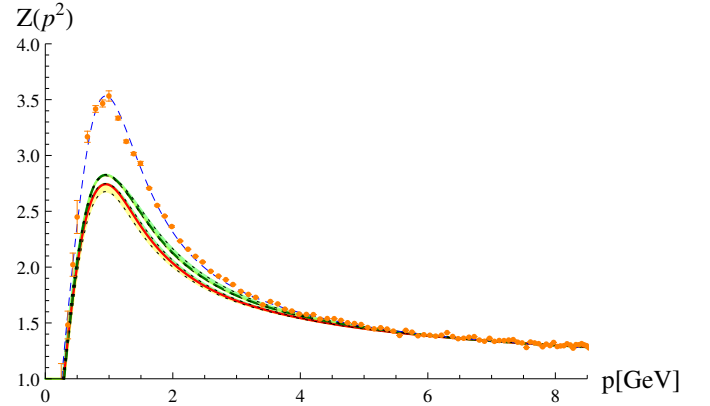


Figure 8: Gluon dressing functions as in Fig. 4, here for $SU(2)$: Input from [7] (dashed blue), lattice data from [23], results with standalone three-gluon vertex DSE solution (solid red with bands), and 3-point complete self-consistent solution (dashed green).

Given that lattice data for the three-gluon vertex is only available for the gauge group $SU(2)$ [26], we also calculated the vertex and the propagators for $SU(2)$. As propagator input we used a solution of the propagator system with a bare ghost-gluon vertex and an optimized three-gluon vertex [7], see blue dashed line in Fig. 8. Also in the three-gluon vertex DSE a bare ghost-gluon vertex was employed, since we know from $SU(3)$, where we checked this explicitly, that this only leads to minor quantitative modifications at a level barely visible in the plots presented here.

As for $SU(3)$ we determine three sets of parameters for the four-gluon vertex model to obtain a band that covers the lattice data, see lower band in Fig. 10. These vertex results were in turn used in the propagator DSEs, where for this calculation a ghost-gluon vertex calculated in the same manner as the three-gluon vertex was employed. The resulting propagator dressings are shown in

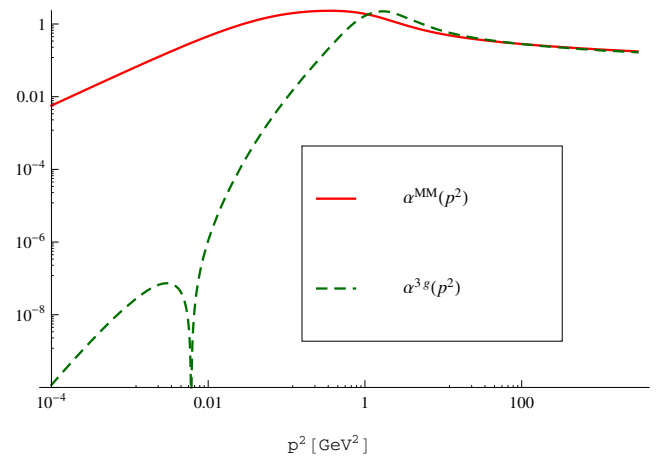


Figure 9: $SU(2)$ couplings obtained from ghost-gluon (solid red) and three-gluon (dashed green) vertices.

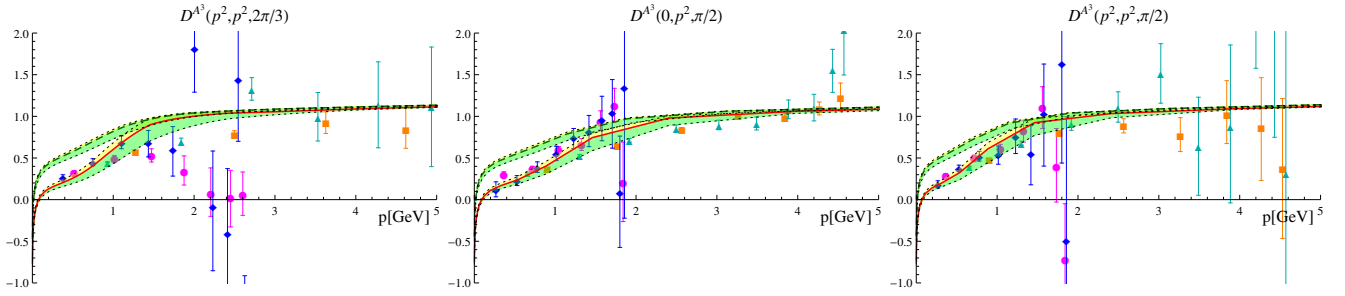


Figure 10: $SU(2)$ three-gluon vertex for three kinematical configurations (as specified above the plots) in comparison with $SU(2)$ lattice data from [26]. Color coding as in Fig. 2, solid red line: standalone vertex DSE solution with $a = 1.5$ and $b = 1.67 \text{ GeV}^2$ in four-gluon vertex model. Corresponding upper (yellow) band: $a = 1.25, b = 1.67 \text{ GeV}^2$; lower (green) band: $a = 1.5, b = 3.34 \text{ GeV}^2$. Dashed green line (here also with bands): fully iterated results from 3-point complete truncation for the same values and ranges of a and b .

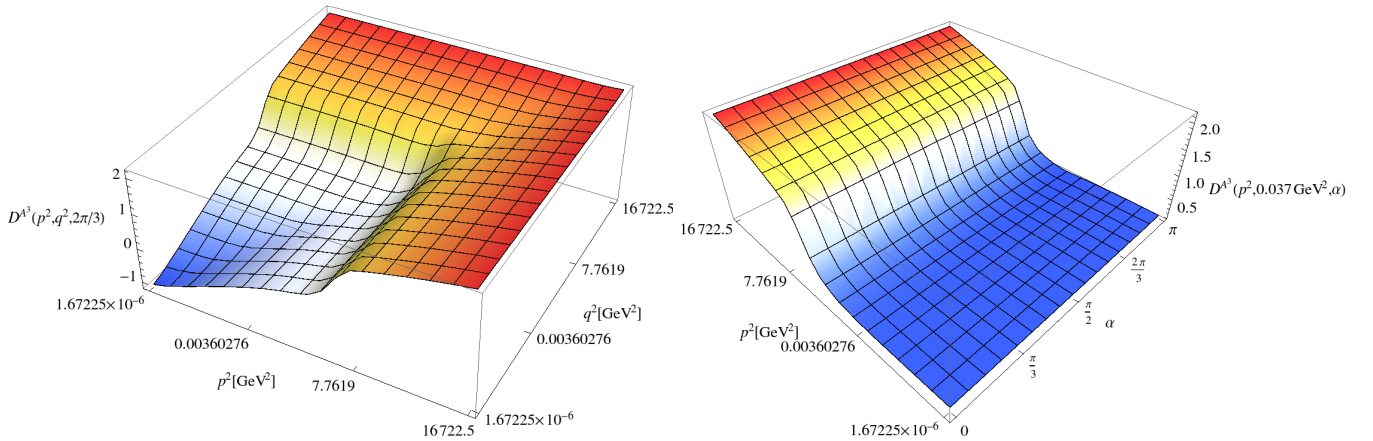


Figure 11: $SU(2)$ three-gluon vertex corresponding to the solid red solution in Fig. 10, but now with two momenta p and q at a fixed angle $\alpha = 2\pi/3$ (left), and for fixed $q^2 = 0.037 \text{ GeV}^2$ but varying angle α (right).

figs. Fig. 8 and Fig. 7. The values for the zero crossings of the three-gluon vertex are $81^{+20}_{-13} \text{ MeV}$, $96^{+17}_{-17} \text{ MeV}$ and $70^{+20}_{-8} \text{ MeV}$ in this case (configurations in the same order as in Fig. 10). The corresponding values for $SU(3)$ are $85^{+34}_{-7} \text{ MeV}$, $100^{+15}_{-7} \text{ MeV}$ and $81^{+26}_{-10} \text{ MeV}$.

For the self-consistent solution we show also a band that corresponds to the same models of the four-gluon vertex. We note that the band from the self-consistent calculation is smaller than that from the three-gluon vertex-only calculations. Furthermore, the bands in the gluon dressing are smaller for $SU(2)$ than for $SU(3)$.

It is possible that this hints at larger deviations from the real vertex for $SU(3)$ than anticipated from the close resemblance of $SU(2)$ and $SU(3)$ propagators. The $SU(2)$ couplings are shown in Fig. 9. In Fig. 11 we present three-dimensional plots of the three-gluon vertex $D^A^3(p^2, q^2, \alpha)$. The shown data corresponds to the red line in the middle of the bands in Fig. 10. The plot with one fixed momentum illustrates that there is only a small angle dependence in the vertex. The same is true for $SU(3)$.